Imaginary deuteron optical potential due to elastic and inelastic breakup

A. Ingemarsson*
The Svedberg Laboratory and Department of Radiation Sciences, Box 533, S-75121 Uppsala, Sweden

R. Shyam†
Saha Institute of Nuclear Physics, Calcutta-700064, India

(Received 28 May 1999; revised manuscript received 3 June 1999; published 18 October 1999)

The contributions to the reaction cross section from elastic and inelastic breakup processes, calculated within the post-form distorted-wave Born-approximation theory, are used as constraints to determine the contributions to the imaginary part of the deuteron optical potential (IPDOP) due to the breakup channels. The Coulomb part of this potential due to the elastic breakup process is seen to account for the long range absorption in the optical potential. The nuclear parts of the IPDOP due to the elastic and inelastic breakup modes peak in different regions of the nuclear surface, with the latter being almost an order of magnitude larger than the former. This makes the IPDOP, due to the breakup channels determined by us, stronger than those calculated earlier ignoring the inelastic breakup mode. [S0556-2813(99)02111-1]

PACS number(s): 24.10.Ht, 25.45.De

I. INTRODUCTION

In collisions between two nuclei the breakup of the projectile into two or more fragments is often a strong reaction channel, which affects not only the imaginary part but also the real part of the corresponding optical potential. This leads to a dynamical polarization potential (DPP) which has to be added to the real potential calculated by double folding models (DFMs) (see, e.g., a recent review in [1]). Otherwise, the real part of the DFM potentials for weakly bound projectiles (e.g., ^{6,7}Li and ^{9}Be) require arbitrary renormalization factors in order to fit their elastic scattering data [2]. Whereas folding model calculations have been performed for both real and imaginary parts of the nucleon optical potentials [3], for the case of light ions they are confined only to the real potentials which together with a phenomenological imaginary part is used to describe the corresponding elastic scattering.

One of the problems associated with the microscopic calculations of the imaginary part of the light ion optical potential has been to include the effects due to breakup of the projectile in the field of the target nucleus, which is a strong reaction channel for these nuclei. Experimental studies have shown that even for strongly bound projectiles the probability of breakup increases drastically with increasing beam energy [4,5]. For example, the cross section for breakup of the α particle into $n+^{3}$He increases by, at least, an order of magnitude as the beam energy is varied from 65 MeV to 140 MeV [6,7]. Thus the effects of breakup are important also for tightly bound projectiles for beam energies above 30 MeV/nucleon.

The optical potentials due to the breakup channels have been calculated by several authors in the past [8–11]. Most of them are based on coupled channel (CC) techniques where the excitation of the breakup channel and its feedback on the elastic channel is studied. However, such calculations are rather complicated as one has to find reliable approximations to include the higher order effects and the complete breakup continuum in the calculations [10,11]. Moreover, the inelastic breakup mode, which dominates the total breakup cross sections [12], cannot be included in these calculations.

In this paper we follow a method introduced in [13], where it was shown that unitarity of the scattering matrix makes it possible to investigate the influence of the breakup process on the elastic scattering even without introducing the coupling of the breakup channel back to the elastic channel. In this procedure, the elastic scattering and breakup reaction are investigated separately. In the first step, the breakup of the projectile in the nuclear and Coulomb fields of the target nucleus is calculated following post-form distorted-wave Born-approximation (DWBA) theory. In this first order theory, which reproduces the experimental breakup data rather well, only the coupling of the elastic channel to the breakup channel is considered. The contribution of each partial wave of the incident projectile to the total breakup cross section can be explicitly determined within this theory. Without such a partial-wave decomposition, the present approach would have not been feasible.

In the second step, the elastic scattering of the projectile is calculated from the known optical potential. We determine the reaction cross section for each partial wave (which are uniquely determined by the imaginary part of the corresponding phase shifts) and split it (using the unitarity of the scattering matrix) into two parts, one due to the breakup channels and the another due to the rest. Since the reaction cross sections out of a specific channel can be related to the expectation value of the imaginary part of the optical potential associated with that channel (which is calculated with the corresponding optical model wave function in the entrance channel) [14], we use the breakup cross sections calculated within post-form DWBA theory as constraints in a fitting procedure to determine the imaginary part of the potential due to the breakup channels. We prefer not to call it the

*Electronic address: Anders.Ingemarsson@tsl.uu.se
†Electronic address: shyam@tnp.saha.ernet.in

dynamical polarization potential as this phrase is used for potentials having both real and imaginary parts.

The formalism used in our calculations is discussed in the next section. The results and their discussions are presented in Sec. III. The summary and conclusions of our work are given in Sec. IV.

II. METHOD OF CALCULATIONS

We write the phenomenologically determined optical potential $U(r)$ $[=V(r)+iW(r)]$ as

$$U(r)=[U(r)-U_{\rm bu}(r)]+U_{\rm bu}(r), \tag{1}$$

where $U_{\rm bu}$ is the dynamical polarization potential due to the breakup channels. The wave functions $y_l(r)$ and $w_l(r)$, corresponding to potentials $U(r)$ and $[U(r)-U_{\rm bu}(r)]$ $[=U_{\rm bare}(r)$, the bare potential], respectively, satisfy the following radial Schrödinger equations:

$$\frac{d^2y_l(r)}{dr^2}+\left[k^2-U(r)-\frac{l(l+1)}{r^2}\right]y_l(r)=0, \tag{2}$$

$$\frac{d^2w_l(r)}{dr^2}+\left[k^2-U_{\rm bare}(r)-\frac{l(l+1)}{r^2}\right]w_l(r)=0, \tag{3}$$

where k is the wave number of the incident deuteron. For $r>R_p$ (where R_p is the distance beyond which the nuclear interactions can be ignored), the wave functions $y_l(r)$ and $w_l(r)$ are normalized according to

$$y_l(r)\sim e^{i\delta_l}[\cos\delta_l F_l(kr)+\sin\delta_l G_l(kr)], \tag{4}$$

$$w_l(r)\sim e^{i\delta_l^0}[\cos\delta_l^0 F_l(kr)+\sin\delta_l^0 G_l(kr)], \tag{5}$$

where F_l and G_l are the regular and irregular Coulomb functions. δ_l and δ_l^0 are the scattering phase shifts corresponding to potentials $U(r)$ and $U_{\rm bare}(r)$.

The expressions for the partial-wave amplitudes can be written in either of the following two forms [15]:

$$f_l=-\frac{1}{k}\int_0^\infty F_l(kr)U_{\rm bare}(r)y_l(r)dr$$

$$-\frac{1}{k}\int_0^\infty F_l(kr)U_{\rm bu}(r)y_l(r)dr=f_l^A+f_l^B \tag{6}$$

and

$$f_l=-\frac{1}{k}\int_0^\infty F_l(kr)U_{\rm bare}(r)w_l(r)dr$$

$$-\frac{1}{k}\int_0^\infty w_l(kr)U_{\rm bu}(r)y_l(r)dr=f_l^C+f_l^D. \tag{7}$$

These decompositions of the partial-wave amplitudes were used in an earlier study [16] of the optical potential due to breakup channels. However, the breakup amplitude was assumed to be obtained from the difference $f_l-f_l^C$ instead of $f_l-f_l^A$. This neglected the fact that the amplitude from the bare potential is affected by the presence of the breakup potential and generated a dependence on the real part of the breakup potential. As will be shown below, a separation of the reaction cross section into contribution of various channels requires knowledge of the real potential $V(r)$ only.

Although the reaction cross section (which includes contributions from all the inelastic channels) can be calculated directly from the partial-wave amplitudes described above, we use here an expression where it is written in terms of the imaginary part of the optical potential [14,17]. This method was used earlier [18,17,19] to calculate the contributions to the imaginary part of the optical potential from the fusion channels. We can write the reaction cross section (σ_R) as

$$\sigma_R=\frac{2\pi}{\hbar v}\langle\chi_i^{(+)}|W|\chi_i^{(+)}\rangle, \tag{8}$$

where v is the relative velocity in the entrance channel and $\chi_i^{(+)}$ the full solution of the Schrödinger equation (whose radial part is y_l). We can also write

$$\sigma_R=\frac{\pi}{k^2}\sum_l (2l+1)T_l, \tag{9}$$

where the transmission coefficient (T_l) is given by

$$T_l=\frac{4}{\hbar v}\int_0^\infty |y_l(r)|^2W(r)dr. \tag{10}$$

It may be noted that T_l can also be related to the amplitudes f_l [Eqs. (6) and (7)] by $T_l=4(|f_l|^2-f_l^I)$, where f_l^I denotes the imaginary part of f_l. However, the advantage of Eq. (10) lies in the fact that it involves a linear dependence of T_l on the imaginary potential. This allows us to split T_l into terms corresponding to the contributions from different channels, as will be discussed below.

Using unitarity of the S matrix, the transmission coefficient T_l can be written as

$$T_l=1-|S_{ll}|^2=\sum_{c\neq l}|S_{lc}|^2, \tag{11}$$

where S represents the scattering matrix and l denotes the elastic channel. For simplicity of notation we take the projectile and target nuclei to be spinless; hence l corresponds to the total spin, and c describes any other channel with total angular momentum l. Thus Eq. (11) enables us to express the transmission coefficient T_l as a sum (or integral for continuous channels) over all the reaction channels. This allows us to write

$$\sigma_R=\sigma_R^{\rm bare}+\sigma_{{\rm bu},d}, \tag{12}$$

for each partial wave l. In this equation $\sigma_{{\rm bu},d}$ represents the contribution to the reaction cross section from the breakup channels, while $\sigma_R^{\rm bare}$ is the reaction cross section corresponding to the remaining channels. Following Refs. [18,19], we decompose the total imaginary potential $W(r)$ into a bare

component and a component due to breakup as $W(r) = W_{\rm bare}(r) + W_{\rm bu}(r)$. Then, expressions similar to Eq. (9) can be written for $\sigma_R^{\rm bare}$ and $\sigma_{{\rm bu},d}$ with corresponding T_l's given by

$$T_l^{\rm bare} = \frac{4}{\hbar v}\int_0^\infty |y_l(r)|^2 W_{\rm bare}(r)\,dr \tag{13}$$

and

$$T_l^{\rm bu} = \frac{4}{\hbar v}\int_0^\infty |y_l(r)|^2 W_{\rm bu}(r)\,dr, \tag{14}$$

where the $W_{\rm bu}$ consists of a part due to the elastic breakup $W_{\rm diss}$ and a part due to the inelastic breakup $W_{\rm inbu}$. In our fitting procedure, potentials $W_{\rm diss}$ and $W_{\rm inbu}$ (with a certain *a priori* assumed form) are varied so that the elastic or inelastic breakup cross sections (calculated within post-form DWBA theory which is described below) are reproduced for each partial wave. We impose the constraint that $W_{\rm bu} \leqslant W$ for all r. Of course, the potentials due to breakup so determined are specific to our breakup cross section and it could be different from such potentials defined by other authors.

It may be noted that the dependence on the real potential entering into the transmission coefficients [Eqs. (10), (13), and (14)] is only through that of the phenomenological optical potential that is used to calculate y_l. In the calculations presented in this paper we assume that this potential is known from the description of the elastic scattering. Thus no information about the real part of the potential due to the breakup channels can be extracted. However, had one started from a real potential calculated within a double folding model, it would have been necessary to include a dynamical polarization potential (having a real part) in order to reproduce both the elastic scattering and breakup probabilities simultaneously. It is also worthwhile to note that if the energy dependence of the imaginary potential is known over a sufficiently large range of energies, the dispersion relations may be helpful in getting the corresponding real potential [20,21].

In the post-form DWBA theory of the inclusive breakup reaction [e.g., $d+A \rightarrow p+X$, to be represented as (d,p)] the total breakup cross section is defined by [12,13]

$$\sigma_{{\rm bu}(d,p)} = \int d\Omega_p dE_p \frac{d^2\sigma(d,p)}{d\Omega_p dE_p}, \tag{15}$$

where $d^2\sigma(d,p)/d\Omega_p dE_p$ is the double differential cross section for the reaction (d,p), which is the sum of the elastic and inelastic breakup modes. The former [where X corresponds to $n+A$(g.s.)] is given by

$$\frac{d^2\sigma({\rm elastic})}{d\Omega_p dE_p} = \rho({\rm phase}) \sum_{l_n m_n} |\beta_{l_n m_n}|^2. \tag{16}$$

Using a zero-range approximation, the amplitude $\beta_{l_n m_n}$ can be written as

$$\beta_{l_n m_n} = D_0 \int d^3r\, \chi_p^{(-)*}\left(\mathbf{k}_p, \frac{A}{A+1}\mathbf{r}\right) F_{l_n}(k_n, r) \times Y^*_{l_n m_n}(\hat{r})\, \chi_d^{(+)}(\mathbf{k}_d, \mathbf{r})\, \Lambda(r) P(r). \tag{17}$$

D_0 is the zero-range constant for the $d \rightarrow p+n$ vertex. Its value has been taken to be 125 MeV fm$^{3/2}$ which is consistent with the known properties of the p-n system. The function $\Lambda(r)$ takes into account finite range effects within the local energy approximation (LEA) [22,23]. We have used the form of $\Lambda(r)$ as that given in [22] with a finite range correction parameter of 0.621, a value used in most of the calculations on deuteron-induced transfer and breakup reactions. $P(r)$ accounts for the nonlocality of the optical potentials. This is calculated by following the method of Perey and Buck [24,23], with the nonlocality parameters of 0.85 in the neutron and proton channels and 0.54 in the deuteron channel.

In Eq. (17), $\chi^{\pm}$ are the optical model wave functions in the respective channels with k's being the corresponding wave numbers. $F_{l_n}(k_n, r)$ is the radial part of the wave function in the $n+A$(g.s.) channel. In Eq. (16), ρ(phase) is the three-body phase-space factor [25,26]. It should be noted that the integrand in Eq. (17) involves three scattering wave functions which are asymptotically oscillatory. This makes the radial integrals involved therein very slowly converging. However, integrals of this kind can be effectively evaluated by using a contour integration method [27,28].

To calculate the cross section for the inelastic breakup process, where X can be any two-body channel of the $B = n + A$ system, we start from a T matrix

$$T_{d,pX} = \langle \Phi_{BX}^{(-)} \chi_p^{(-)} | V_{np} | \phi_A \phi_d \chi_d^{(+)} \rangle, \tag{18}$$

where ϕ_A and ϕ_d denote the ground state wave functions of the target nucleus A and the projectile (deuteron), respectively. $\Phi_{BX}^{(-)}$ represents the complete scattering state of the system B with the boundary condition X. The integration over the internal coordinates of ϕ_A in Eq. (18) leads to a form factor for the inelastic process. The calculation of the form factor simplifies greatly if we use a surface approximation [29], where we assume that the main contribution to $T_{d,pX}$ comes from the region outside the range of the nuclear interaction. The validity of this approximation has been tested by Kasano and Ichimura [30] by evaluating this integral without recourse to this approximation. These authors find that the surface approximation is valid for the deuteron-induced breakup reaction even at the lower beam energy of 25 MeV. Thus we can represent the radial part of the form factor $(F_{l_n}^X)$ by its asymptotic form

$$F_{l_n}^X = \delta_{l_n X} j_{l_n}(k_n r) + \frac{1}{2}\sqrt{\frac{m_n k_n}{m_X k_X}}(S_{l_n X} - \delta_{l_n X}) h_{l_n}^{(+)}(k_n r), \tag{19}$$

where j_{l_n} and $h_{l_n}^{(+)}$ denote the spherical Bessel and Hankel functions, respectively. $S_{l_n l_n}$ are the scattering matrix elements for the elastic channel corresponding to the angular

momentum l_n. Now, it is straightforward to carry out the integrations over the angles of the unobserved particle to get the double differential cross section from the triple differential cross sections. This leads to a reduced T matrix for the process $d+A\rightarrow p+X$,

$$\tilde{T}_{d,pX}=\sqrt{\frac{m_n k_n}{m_X k_X}}\frac{S_{l_n X}}{S_{l_n l_n}-1}D_0\int d^3r\,\chi_p^{(-)*}\times\left(\mathbf{k}_p,\frac{A}{A+1}\mathbf{r}\right)[F_{l_n}(k_n,r)-j_{l_n}(k_n r)]\times Y^*_{l_n m_n}(\hat{r})\chi_d^{(+)}(\mathbf{k}_d,\mathbf{r})\Lambda(r)P(r). \quad (20)$$

In order to calculate the double differential cross section for the inelastic breakup, one has to sum over all the channels $X\neq l_n$. Since in Eq. (20) the entire dependence on channel X rests solely in the S matrix $S_{l_n X}$, this summation can be easily carried out using the unitarity of the S matrix:

$$\sum_{X\neq l_n}|S_{l_n X}|^2=1-|S_{l_n l_n}|^2. \quad (21)$$

Therefore, we only need to know the S-matrix elements of the elastic scattering to determine the double differential cross sections for the inelastic breakup, which can be written as

$$\frac{d^2\sigma(\text{inelastic})}{d\Omega_p dE_p}=\rho(\text{phase})\times\sum_{l_n m_n}(\sigma_{l_n}^{\text{reaction}}/\sigma_{l_n}^{\text{elastic}})|\beta_{l_n m_n}-\beta^0_{l_n m_n}|^2. \quad (22)$$

In this equation $\sigma_{l_n}^{\text{reaction}}$ and $\sigma_{l_n}^{\text{elastic}}$ are the reaction and elastic scattering cross sections for the neutron-target system corresponding to the partial wave l_n, respectively. $\beta^0_{l_n m_n}$ is defined in the same way as Eq. (17) with the wave function F_{l_n} being replaced by the spherical Bessel function. More details of the derivation of the inelastic breakup cross sections can be found in Refs. [12,29].

The total cross section for the reaction (d,p) can also be written as

$$\sigma_{\text{bu}(d,p)}=\frac{\pi}{k^2}\sum_l(2l+1)T_l^{\text{bu}(d,p)}, \quad (23)$$

where $T_l^{\text{bu}(d,p)}$ is the transmission coefficient for the (d,p) breakup reaction, which is also termed as the breakup probability in [13]. The total breakup probability $T_l^{\text{bu},d}$ is given by

$$T_l^{\text{bu},d}=T_l^{\text{bu}(d,pn)}+T_l^{\text{bu}(d,p)}(\text{inelastic})+T_l^{\text{bu}(d,n)}(\text{inelastic}). \quad (24)$$

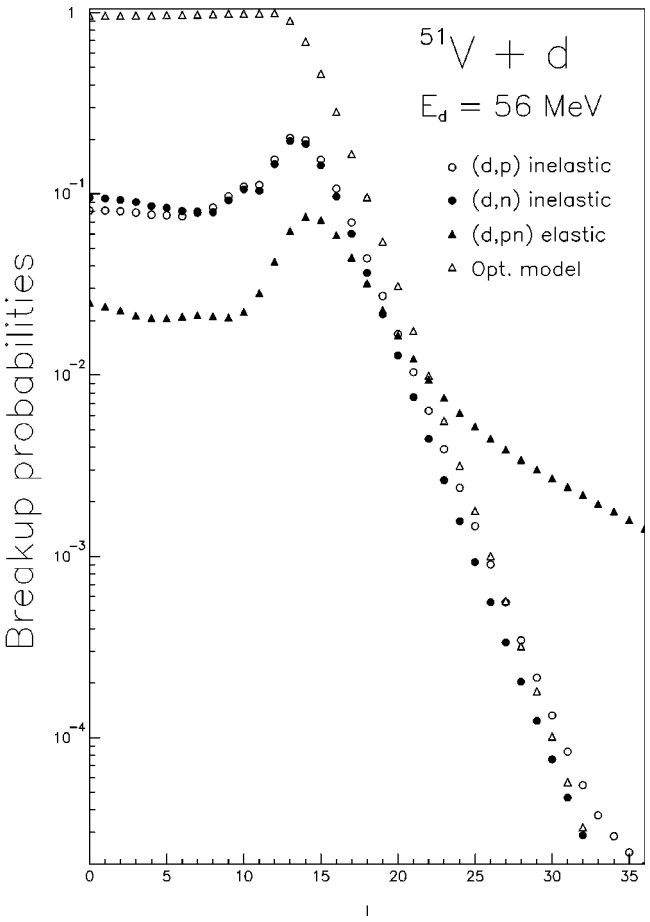

FIG. 1. Calculated breakup probabilities in the scattering of 56 MeV deuteron from ^{51}V. The open triangles show the transmission coefficients calculated with the optical model potential as explained in the text.

In Eq. (24), $T_l^{\text{bu}(d,pn)}$ represents the breakup probability for the elastic breakup mode as defined above. The total breakup cross section $\sigma_{\text{bu},d}$ is obtained from $T_l^{\text{bu},d}$ by following an expression similar to Eq. (9).

III. RESULTS AND DISCUSSION

Apart from the zero-range constant, finite range, and nonlocality parameters described already in Sec. II, we require the optical potentials in the deuteron, proton, and neutron channels to calculate the breakup cross sections. These have been taken from the global sets given by Daehnick, Childs, and Vrcelj [31] (for the deuteron channel) and Becchetti and Greenlees [32] (for the proton and neutron channels), respectively.

In Fig. 1 we show the results for the breakup probability for the deuteron incident on a ^{51}V target at the beam energy of 56 MeV, calculated within post-form DWBA theory. In this figure we have also shown the total transmission coefficients calculated with the same deuteron optical potential. We can see that the (d,p) and (d,n) breakup probabilities are similar in shape and absolute magnitude. The elastic breakup probability is much smaller and shows a different

behavior as a function of l. The cross sections for the inelastic (d,p), inelastic (d,n) and elastic (d,pn) breakup processes are 290 mb, 284 mb, and 122 mb, respectively, which lead to a total deuteron breakup cross section of 698 mb for this target. The total (d,p) breakup cross section [which is the sum of inelastic (d,p) and elastic (d,pn) cross sections] is 412 mb which is in reasonable agreement with the measured value of 481 mb [33]. The remaining difference between the experimental and theoretical cross sections, to some extent, may be attributed to the likely contributions of quasielastic channels like (d,dp) to the inclusive proton spectra.

An important feature of Fig. 1 is the fact that for $l>21$, the elastic breakup probability (EBP) exceeds the total transmission coefficient. This shows the inadequacy of the phenomenological deuteron optical potential (used to determine the transmission coefficient) for larger values of l. The Woods-Saxon shapes used to obtain such optical potentials are too restricted in their radius dependence. It is obvious that these potentials do not account correctly for the elastic breakup channel (which we shall refer to as dissociation in the following) at large distances. We also note from this figure that both elastic and inelastic breakup probabilities are relatively large at very small partial waves. This is the consequence of the weak absorption of neutrons and/or protons. For breakup reactions involving heavier projectiles, these probabilities are quite small at these partial waves [12,13].

Now we proceed to determine the potential due to the dissociation process. As already pointed out in Ref. [13], it is the Coulomb force which is responsible for the long range part of the EBP. In case of a pure Coulomb interaction, the eikonal approximation may be used to relate the imaginary phase shifts to an imaginary potential [34,35]. Since $\sigma_{\mathrm{bu},d}$ defines uniquely an imaginary phase shift, we can use this method to determine the imaginary pure Coulomb dissociation potential by fitting the EBP calculated by post-form DWBA theory with Coulomb interactions only between the deuteron and proton and the target nucleus.

On the left side of Fig. 2, the Coulomb EBPs are shown with Coulomb interactions obtained from (1) an uniform charge distribution [with a radius (R_C) of 1.3 fm] (solid circles) and (2) a Woods-Saxon charge distribution with radius and diffuseness parameters of 1.3 fm and 0.65 fm, respectively (open circles). We observe that the Coulomb dissociation is sensitive to the charge distribution for small l values. For larger partial waves, however, they produce identical results which is to be expected. It is explicitly clear (together with Fig. 1) that the Coulomb force determines the EBP at higher partial waves. We have used an EBP calculated with the Coulomb potentials generated from the Woods-Saxon charge distribution to perform the fits. In fact, this diffuse Coulomb potential has been used in all the post-form DWBA calculations presented in this paper.

We used a two-parameter, (ae^{-br}) as well as a six-parameter parametrization $[(a_1+a_2r^{1/2}+a_3r+a_4r^5)/(1+a_4r)]e^{(-b_1r-b_2r^2)}$ in our fitting process. The best fit breakup probabilities obtained with the two procedures are shown by dotted and solid curves in the left part of Fig. 2. The corresponding imaginary potentials are shown in the right side of this figure. The six-parameter search procedure (with b_1 and b_2 being equal to 0.1118 and 0.0113) provides a better fit to the EBP. The two-parameter fits had a radial dependence of $e^{-0.3r}$. In comparison to this the Woods-Saxon potential behaves approximately as $e^{-r/a}\approx e^{-2.0r}$ (with a being the diffuseness parameter), at larger distances. Therefore, it is not surprising that the transmission coefficients calculated with conventional optical potentials drop too fast at larger partial waves.

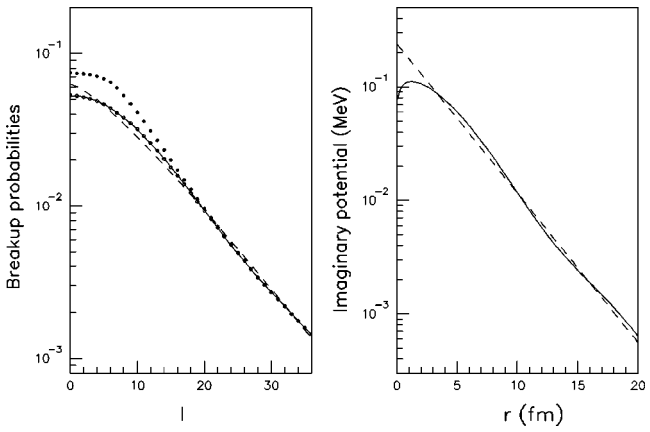

FIG. 2. Results of calculations without nuclear interactions. The left part of the figure shows the calculated Coulomb elastic breakup probabilities for the same reaction as in Fig. 1 obtained with Coulomb potentials generated with a uniform charge distribution (solid circles) and a charge distribution with Woods-Saxon shape (open circles). The dashed and solid curves show the best fits obtained by using two and six parameter parametrizations. The right part shows the corresponding best fit potentials obtained by fitting to the breakup probability calculated with the Woods-Saxon charge distribution. The solid (dashed) curve represents the results obtained with six- (two-) parameter parametrizations.

It is clear that the potential due to the Coulomb dissociation (PCD) is very weak. We found that the elastic scattering angular distributions calculated with phenomenological optical potential were almost unaffected by inclusion of the PCD to its imaginary part. Also this leads to a change of less than 1% in the total reaction cross section. The transmission coefficients at lower partial waves are affected by the inclusion of the PCD, but the nuclear effects damp them out strongly in this region, as is discussed in the context of Fig. 3.

We therefore added the PCD to the phenomenological imaginary potential as it leads to a total transmission coefficient which is larger than (or equal to) the EBP for all partial waves as can be seen from the left part of Fig. 3, where the total transmission coefficients obtained with (solid triangles) and without (open triangles) adding the PCD to the phenomenological optical potential are shown. It can be seen that the addition of the PCD to the phenomenological potential removes the anomaly described above. In the right side of Fig. 3, we compare the results of the Coulomb EBP obtained with [by using Eq. (13)] and without nuclear distortion. We note that nuclear distortion effects suppress the Coulomb EBP strongly for lower partial waves. However, for larger partial waves the two calculations produce identical results.

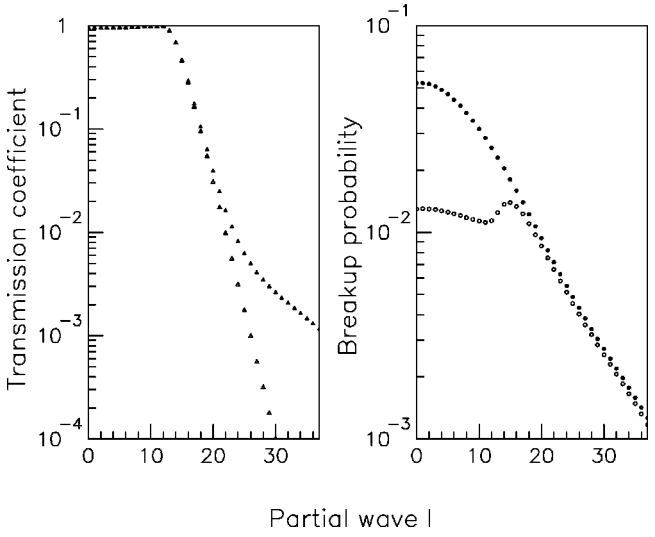

FIG. 3. The left part shows the transmission coefficients in the elastic scattering calculated with the phenomenological optical potential with (solid triangles) and without (open triangles) the addition of the imaginary potential due to elastic Coulomb dissociation. The right part shows the breakup probabilities for elastic Coulomb dissociation calculated in the eikonal approximation (same curve as shown in Fig. 2) (solid circles) and those obtained in the full calculations with nuclear distortions included (open circles).

In order to find the potentials due to the inelastic breakup and nuclear dissociation, we used Eq. (13). The inelastic and elastic breakup probabilities calculated within the post form DWBA (Fig. 1) were fitted by using a sum of Gaussians (SOG) parametrization [36]

$$U_{\rm bu}^{\rm SOG}(r)=\sum_i A_i(\exp[-\{(r-R_i)/\gamma\}^2] + \exp[-\{(r+R_i)/\gamma\}^2]). \quad (25)$$

The value of γ was taken to be $\sqrt{2/3}$ [36], and a total of 15 terms were included in the sum. The coefficients A_i and positions R_i were varied in order to get the best fits to the elastic, inelastic, and total breakup probabilities, which are shown, in the left, middle, and right parts of Fig. 4, respectively. The solid circles show the results of the post-form DWBA (same as that in Fig. 1), while open circles represent our fits. In case of the EBP, we also show the results for the pure Coulomb case (open triangles) (the same as shown in the right side of Fig. 2). We can see that the Coulomb EBP agrees very well with that obtained by fitting the total EBP for values of $l > 21$. It should be remarked here that in the study of Christley *et al.* [19], who have used a similar method to determine the fusion potential by fitting to the fusion cross sections calculated within a coupled-reaction-channel model, the quality of fits were not as good. They attribute this failure to the lack of l dependence in their fitting potential (which were taken to be of the Woods-Saxon type). However, we do not require such a dependence in our fitting procedure.

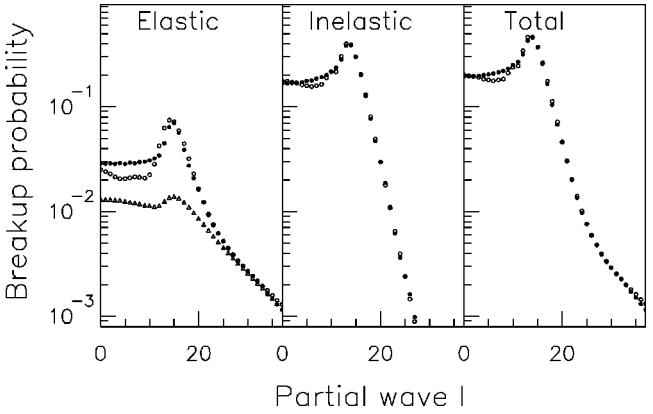

FIG. 4. The elastic, inelastic, and total breakup probabilities calculated within the post-form distorted-wave Born approximation (solid circles) and our best fit values to them (open circles). Open triangles, in the left part of the figure, represent the breakup probability for the elastic Coulomb dissociation (same as those shown in the right part of Fig. 3 by open circles).

The potentials giving these breakup probabilities are shown in the upper part of Fig. 5. The solid, dashed, and dotted curves show the potentials due to the inelastic breakup (which has been plotted after multiplying the actual values by 0.09), nuclear dissociation, and Coulomb dissociation (already shown in Fig. 2), respectively. We note that the inelastic breakup and nuclear dissociation potentials are strongly concentrated in a region around 6.5 fm and 8 fm, respectively. Both potentials have about the same width, 2 fm [full width at half maximum (FWHM)], which is very similar to the rms radius of the deuteron. The difference in the localization of the inelastic and dissociation potentials confirms the fact that inelastic breakup of the projectile occurs in regions closer to the target nucleus as compared to the elastic breakup. It is worthwhile to note that the potential due to the inelastic breakup is quite large. Therefore, those calculations [10,11,37,38] where this mode of breakup is not considered are likely to produce weaker imaginary potentials due to the breakup channels as compared to ours. Because of its long range, the potential due to the Coulomb dissociation is still of appreciable magnitude at large distances. Coulomb breakup thus can take place even outside the charge distribution of the target nucleus.

In the middle part of Fig. 5, we compare the imaginary part of the phenomenological optical potential (solid line) with the bare potential (obtained by subtracting the potential due to breakup from it) (dashed line). It is clear that breakup is the dominant absorption effect in the surface region. The bare potential could be the starting point of double folding model calculations.

In the lower part of Fig. 5, we show the radial dependences of the neutron, proton, and matter densities for the ^{51}V nucleus [39]. We note that breakup potentials peak in a region where the matter and charge densities are much

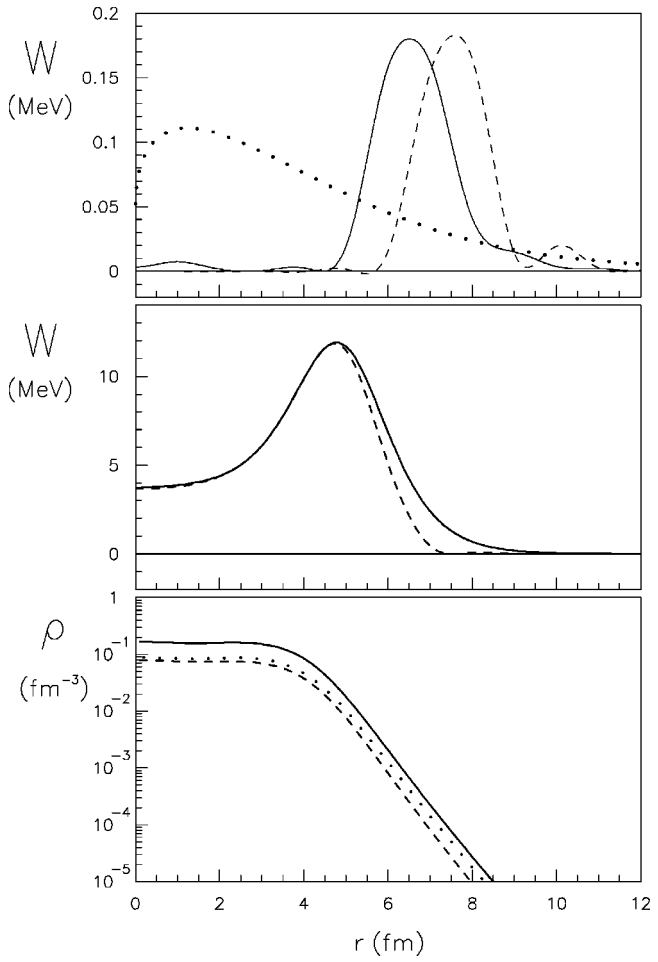

FIG. 5. The upper figure shows the imaginary potentials due to inelastic breakup (arbitrarily multiplied by 0.09 to fit in the plot) (solid line) and the potential due to nuclear dissociation (dashed line). The dotted curve shows the Coulomb dissociation potential. The middle part shows the optical potential with (solid curve) and without (dotted curve) effects of breakup. In the lower part the dashed, dotted, and solid curves show the neutron, proton, and matter densities for ^{51}V, respectively, as calculated by Fayans [39].

smaller as compared to the central density of the target nucleus. Therefore, the breakup process is really sensitive to the extreme peripheral regions. This also confirms the spectator role of the target nucleus in the breakup process (Serber picture). However, the region where the breakup potentials peak is much larger than the half density radius deduced by Serber [40]. This could be of interest for the reactions of neutron halo nuclei.

It should be stressed that our method of obtaining the imaginary part of the optical potential due to the breakup channels is phenomenological in nature. However, it has several good features. The distinctly different nature of the total breakup cross section as a function of the incident partial waves is automatically taken into account. The Coulomb breakup process which is responsible for the long range part of the elastic breakup probability (and the dissociation potential) is included into our calculations. Furthermore, we include the inelastic breakup mode which makes the largest contribution to the imaginary potential. Both these effects were ignored in calculations presented in Refs. [10,11].

IV. SUMMARY AND CONCLUSIONS

In this paper we calculated the imaginary part of the optical potential due to the breakup channels by using a phenomenological method in which contributions to the reaction cross sections from the elastic and inelastic breakup cross sections of the projectile in the field of target nuclei, calculated in the post-form distorted-wave Born approximation, are used as constraints in a fitting procedure. In this method, only the first order breakup process (the coupling of the elastic channel to the breakup channel) is considered. Then unitarity of the *S* matrix is used to determine the influence of breakup on the elastic channel.

The Coulomb part of the imaginary dissociation potential (obtained from the pure Coulomb elastic breakup probabilities) accounts for the long range part of the absorption and removes the anomaly where for partial waves beyond 20 the elastic breakup probabilities were found to be even larger than the transmission coefficients calculated with the usual phenomenological optical potentials. To our knowledge this is the first calculation where the absorption due to the Coulomb dissociation process has been included in the optical model. The potentials due to the nuclear dissociation are found to be peaked in the region around 8.0 fm.

The imaginary potential due to inelastic breakup is about an order of magnitude larger than that due to the dissociation process, and is concentrated at somewhat shorter distance (around 6.5 fm) as compared to the latter. This suggests that inelastic breakup takes place at distances closer to the target nucleus in comparison to elastic breakup. The magnitude of the total imaginary potential, due to the breakup channels (IPBC), is, therefore, almost solely due to the inelastic breakup process in the region around 6–8 fm. This is consistent with the dominant contribution of this mode to the total breakup cross section. This is the main reason for our IPBC being stronger than the imaginary part of the dynamical polarization potential due to breakup channels calculated by other authors, who have ignored the inelastic breakup mode.

Our method can be applied to any projectile having a strong breakup channel. Therefore, it would be interesting to use this method to the elastic scattering of halo nuclei (e.g., ^{11}Li and ^{11}Be) [41], where the breakup cross sections are significantly enhanced and the effect of breakup on the elastic scattering is very strong.

ACKNOWLEDGMENTS

This work has been supported by the Wenner-Gren Center Foundation, Stockholm. One of the authors (R.S.) would like to acknowledge several useful discussions with Professor I.J. Thompson of the University of Surrey, Guildford. We also want to thank Sergei Fayans for providing the densities for ^{51}V.

[1] M. E. Brandan and G. R. Satchler, Phys. Rep. **285**, 143 (1997).
[2] G. R. Satchler and W. G. Love, Phys. Rep. **55**, 183 (1979).
[3] G. Fäldt and A. Ingemarsson, J. Phys. G **9**, 261 (1983).
[4] J. R. Wu, C. C. Chang, and H. D. Holmgren, Phys. Rev. Lett. **40**, 1013 (1978).
[5] A. Budzanowski *et al.*, Phys. Rev. Lett. **41**, 635 (1978).
[6] R. J. de Meijer, E. H. L. Aarts, M. B. Greenfield, and W. A. Sterrenburg, Nucl. Phys. **A402**, 15 (1983).
[7] R. W. Koontz, C. C. Chang, H. D. Holmgren, and J. R. Wu, Phys. Rev. Lett. **43**, 1862 (1979).
[8] I. J. Thompson and M. A. Nagarajan, Phys. Lett. **106B**, 163 (1981).
[9] H. Amakawa, A. Mori, H. Nishioka, K. Yazaki, and S. Yamaji, Phys. Rev. C **23**, 583 (1981).
[10] Y. Sakuragi, M. Yahiro, and M. Kamimura, Prog. Suppl. Theor. Phys. **89**, 136 (1986).
[11] K. Yabana, Y. Ogawa, and Y. Suzuki, Phys. Rev. C **45**, 2909 (1992); Nucl. Phys. **A539**, 295 (1992).
[12] G. Baur, F. Rösel, D. Trautmann, and R. Shyam, Phys. Rep. **111**, 334 (1984).
[13] G. Baur, R. Shyam, F. Rösel, and D. Trautmann, Phys. Rev. C **21**, 2668 (1980); Helv. Phys. Acta **53**, 506 (1980).
[14] M. S. Hussein and K. W. McVoy, Nucl. Phys. **A445**, 124 (1985).
[15] L. S. Rodberg and R. M. Thaler, *Introduction to the Quantum Theory of Scattering* (Academic Press, New York, 1967).
[16] A. Ingemarsson, Phys. Rev. C **55**, R1023 (1997).
[17] T. Udagawa, B. T. Kim, and T. Tamura, Phys. Rev. C **32**, 124 (1985).
[18] M. S. Hussein, Phys. Rev. C **30**, 1962 (1984).
[19] J. A. Christley, M. A. Nagarajan, and I. J. Thompson, J. Phys. G **17**, L163 (1991).
[20] M. A. Nagarajan, C. C. Mahaux, and G. R. Satchler, Phys. Rev. Lett. **54**, 1136 (1985).
[21] C. Mahaux, H. Ngô, and G. R. Satchler, Nucl. Phys. **A449**, 354 (1986).
[22] P. J. A. Buttle and L. J. B. Goldfarb, Proc. Phys. Soc. London **83**, 701 (1964).
[23] G. R. Satchler, *Direct Nuclear Reactions* (Oxford University Press, New York, 1983).
[24] F. G. Perey and B. Buck, Nucl. Phys. **A32**, 353 (1962).
[25] G. G. Ohlsen, Nucl. Instrum. Methods **37**, 240 (1965).
[26] H. Fuchs, Nucl. Instrum. Methods Phys. Res. **200**, 361 (1982).
[27] C. M. Vincent and H. T. Fortune, Phys. Rev. C **2**, 782 (1970).
[28] K. T. R. Davis, M. R. Strayer, and G. D. White, J. Phys. G **14**, 961 (1988).
[29] J. Pampus, J. Bisplinghoff, J. Ernst, T. Mayer-Kuckuk, J. Rama Rao, G. Baur, F. Rösel, and D. Trautmann, Nucl. Phys. **A311**, 141 (1978).
[30] A. Kasano and M. Ichimura, Phys. Lett. **115B**, 81 (1982).
[31] W. W. Daehnick, J. D. Childs, and Z. Vrcelj, Phys. Rev. C **21**, 1153 (1980).
[32] F. D. Becchetti and G. W. Greenless, Phys. Rev. **182**, 1190 (1969).
[33] N. Matsuoka, M. Kondo, A. Shimizu, T. Saito, S. Nagamachi, H. Sakaguchi, A. Goto, and F. Ohtani, Nucl. Phys. **A345**, 1 (1980).
[34] G. R. Satchler, *Introduction to Nuclear Reactions*, 2nd ed. (MacMillan, London, 1990).
[35] A. Ingemarsson, Phys. Rev. C **56**, 950 (1997).
[36] H. De Vries, C. W. De Jager, and C. De Vries, At. Data Nucl. Data Tables **36**, 495 (1987).
[37] G. Baur and D. Trautmann, Phys. Rep. **25**, 294 (1976).
[38] G. F. Bertsch, B. A. Brown, and H. Sagawa, Phys. Rev. C **39**, 1154 (1989).
[39] S. A. Fayans, JETP Lett. **68**, 169 (1998).
[40] R. Serber, Phys. Rev. **72**, 1008 (1947).
[41] J. J. Kolata *et al.*, Phys. Rev. Lett. **69**, 2631 (1992).